Synthesis, characterization and enhanced photocatalytic activity of lanthanum doped ZnO nanospheres

XIAOWEN HE, CHANGZHEN LIU, XIAOHONG YU, DAWEI MENG*, JUNFEI CHEN, CAN LU, XIULING WU*
Faculty of Materials Science and Chemistry, Engineering Research Center of Nano-Geo Materials of Ministry of Education, China University of Geosciences, Wuhan 430074, China

La-doped ZnO nanospheres (NSs) with different doping concentrations were successfully synthesized via a two-step facile co-precipitation method using oxalic acid and ammonia as precipitation agents. The results revealed that the as-synthesized samples maintained the hexagonal wurtzite structure until the dopant content reached 1.5 at.%, and La doping resulted in a significant particle size reduction. The band gap increased from 3.163 to 3.193 eV with the increase of La content from 0.5 to 1.5 at.%. The photocatalytic activity for degradation of methyl orange (MO) revealed that photocatalysts with La^{3+} incorporation had much higher photo-degradation efficiency than undoped ZnO. The enhanced photocatalytic performace was correlated with the increase of band gap, which promoted the generation of highly reactive radicals in the surface of ZnO. Other equally important contributor was the uniform nanoscale surface morphology, which improved the adsorption performance of MO on the surface of La-doped ZnO NSs.

(Received January 13, 2014; accepted July 10, 2014)

Keywords: La-doped ZnO, Co-precipitation, Energy band gap, Photocatalytic degradation

1. Introduction

Over the decades, the excessive pursuit of economic growth has resulted in lots of environmental issues, with discharge of industrial wastewater containing dyestuffs being considered as one of the big threats [1-3]. Great efforts have been made in order to eliminate the chemically stable contaminants from aquatic systems [4]. And photocatalytic degradation has been regarded as a very promising approach by trial and error [5-7]. Among many photocatalysts, ZnO is well-recognized for its physical and chemical stability, high oxidative capacity, nontoxicity and low cost [8-12]. However, in spite of its various advantages, the application of ZnO as photocatalyst has been limited by the fast recombination rate of photo-generated electron-hole pairs and low quantum yield in the photocatalytic reaction in aqueous solutions [13]. Therefore, doping method has been introduced by researchers as a useful tool to suppress the photo-excited electron-hole recombination and finally improve the photocatalytic performance of ZnO [14, 15]. This is because the dopant sites, defects induced and level structures changed by doping have remarkable impacts on the optical properties and photocatalytic activity of ZnO nanostructures [16]. As for the dopant, rare earth (RE) has been attracting wide attention for its unique 4f-5d and 4f-4f electron transition [17]. It was reported about the higher photocatalytic degradation efficiency exhibited by RE-doped ZnO materials [18, 19]. As the size and morphology of the particles have significant influence over their various properties, researchers have been investigating ways to improve the properties by changing them [20, 21]. Lanthanum doping has shown its advantage in this regard, for it can block the grain growth and agglomeration of ZnO, and dramatically decrease the particle size, thus enhancing the photocatalytic efficiency [22].

The conventional method to synthesize doped ZnO is co-precipitation by using ammonia as precipitant, because ammonia plays a critical role in controlling the morphology and particle size [23]. However, it also has some drawbacks such as low utilization and low yield, which impede the commercialization of the photocatalytic degradation process. Oxalic acid has already been known in the field of metal oxide materials fabrication, since it can help simplify the synthesis process, decrease the cost and not least, produce more homogeneous products [24]. In order to find a cost-effective and highly productive synthesis approach, a two-step facile chemical co-precipitation method by using oxalic acid and ammonia as the precipitants was proposed in this paper in view of the above-mentioned merits of both them. By combining the oxalic acid and ammonia, the ionization process will be promoted and more ZnO samples will be obtained, thus increasing the utilization of the precipitants compared to the conventional methods.

In this study, the mentioned two-step co-precipitation method was applied for the preparation of pure ZnO and La-doped ZnO NSs with various doping concentrations. This approach has seldom been reported, up to now, for

the fabrication of doped ZnO. The effects of La content on the structural, optical properties were discussed in details and particular attention was given to the photocatalytic activity on the degradation of MO.

2. Experimental details

2.1. Materials

Zinc acetate dihydrate ($Zn(Ac)_2 \cdot 2H_2O$) (Analytical grade, Aladdin, China) and lanthanum nitrate hexahydrate ($La(NO_3)_3 \cdot 6H_2O$) (Analytical grade, Aladdin, China) were used as zinc and lanthanum sources, respectively. Oxalic acid ($H_2C_2O_4 \cdot 2H_2O$), ammonia ($NH_3 \cdot H_2O$), ethyl alcohol (CH_3CH_2OH) and methyl orange (MO) were received from Sinopharm Chemical Reagent Co., Ltd., China. All the reagents were in analytical grade and used directly without further purification. Deionized water is used throughout all processes.

2.2. Synthesis of photocatalyst

Pure ZnO and La-doped NSs were prepared by co-precipitation method using oxalic acid and ammonia as precipitation agents. Zinc acetate dihydrate ($Zn(Ac)_2 \cdot 2H_2O$) and lanthanum nitrate hexahydrate ($La(NO_3)_3 \cdot 6H_2O$) were dissolved in deionized water to get 0.5 mol/L solution with the stoichiometric amount of La/Zn=0, 0.2, 0.5, 0.8, 1.0 and 1.5 at.%, respectively. This solution was kept at 80 °C for 0.5 h under magnetic stirring. Afterwards, 1.0 mol/L oxalic acid solution was added into the previous solution under constant stirring until to get a pH value reached to 1. The white precipitates were obtained and they were still stirred rigorously at 80 °C for 1.5 h. Then, ammonia was added dropwise to the suspension under constant stirring until the pH reached 9. The mixtures were still stirred rigorously at 80 °C for 1.5 h. After being cooled to room temperature, the precipitate was recovered by filtration and washed with deionized water and ethanol several times. The solid product was initially dried at 105 °C for 5 h and subsequently annealed at 900 °C in air for 2 h. Finally, pure ZnO and La-doped ZnO with different concentrations were obtained.

2.3. Photocatalyst characterization

The structural measurements of the obtained samples were carried out using a Dmax-3b diffractometer with nickel-filtered Cu Kα (λ=0.15406 nm) radiation (XRD, X' Pert PRO MPD). The field-emission scanning electron microscopy was used for the observation of surface morphology (FESEM, Hitachi SU8010). The surface composition and valence states were measured by an X-ray photoelectron spectroscopy (XPS, VG Multilab 2000). The optical absorption spectra of samples were recorded in the range of 250~800 nm on an ultraviolet-visible spectrophotometer (UV-vis, Shimadzu UV2550).

2.4. Photocatalytic test

The photocatalytic performances of pure ZnO and La-doped ZnO samples were evaluated by the degradation of methyl orange (MO) aqueous solution under UV light irradiation. 0.01 g pure ZnO and La doped ZnO NSs were mixed with 50 mL MO (10 mg/L) aqueous solution in a quartz photochemical reactor tube under ultrasound treatment, respectively. The obtained suspension was stirred in the dark for 20 min until the absorption equilibrium was reached. Then, at given time intervals, the suspension was illuminated under UV light (250 W, 365 nm) for 30 min while under continuous magnetic stirring. The MO aqueous solution was then separated from the catalysts by centrifugation. A UV-1801 spectrophotometer was used to determine the variation of MO concentration by recording the absorption intensity centering at 464 nm. Then the photocatalytic degradation rates of pure ZnO and La-doped ZnO catalysts could be obtained by comparing the absorbance of MO aqueous solution before and after irradiation.

3. Results and discussion

3.1. Structural and compositional analysis

The XRD patterns of pure ZnO and La-doped ZnO NSs are presented in Fig. 1. It can be seen that all La-doped ZnO samples exhibit characteristic peaks corresponding to the hexagonal wurtzite phase of pure ZnO (JCPDS card No: 36-1451) before the doping concentration reached 1.5 at.%. At this point, La_2O_3 appears as a minor phase (marked with '♦') together with the dominant hexagonal phase ZnO. In this investigation, the wurtzite structure of ZnO samples remains unchanged for the doping concentration from 0.2 at.% to 1.0 at.%, inferring that lanthanum ions have been incorporated into the ZnO lattice [17]. The intensity of the diffraction peaks decreases for the doped samples, which indicates that the crystallinity of ZnO has weakened due to La doping. For the 1.0 at.% La-doped ZnO, the full-width at half-maximum (FWHM) of the peaks have been obviously broadened, implying that the incorporated La atoms hinders grain boundary movement and impedes the growth of crystal grains of ZnO [19]. The inset of Fig. 1 represents a partial enlarged drawing of XRD patterns in the range of 34.0°~35.0°. It can be observed that all diffraction peaks slightly shift to a lower degree with the increase of La content, indicating lanthanum ions (0.106 nm) with a radius larger than that of zinc ions (0.074 nm)

have probably been incorporated into the ZnO lattice. The lattice parameters (*a* and *c* axes of the lattice) and the unit cell volume of various La-doped ZnO samples are presented in Table 1. The refined data show that lattice parameters *a* and *c* increase slightly with La dopant. Such variation could be attributed to the substitution of La ions for Zn site or La ions entering into the interstitial lattice [25].

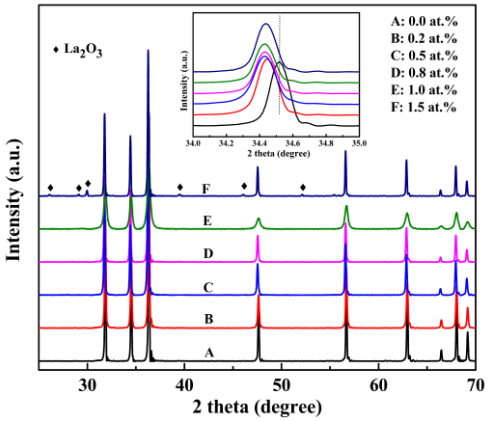

Fig. 1. X-ray diffraction patterns of La-doped ZnO with various doping concentrations.

Table 1. Refined lattice parameters of pure ZnO and La-doped ZnO photocatalysts.

Photocatalysts	Lattice paramater *a* (nm)	Lattice paramater *c* (nm)	Unit cell volume *v* (nm^3)
Pure ZnO	0.3243	0.5196	0.04734
0.2 at.% La-ZnO	0.3249	0.5204	0.04757
0.5 at.% La-ZnO	0.3251	0.5209	0.04768
0.8 at.% La-ZnO	0.3252	0.5210	0.04772
1.0 at.% La-ZnO	0.3253	0.5211	0.04775
1.5 at.% La-ZnO	0.3251	0.5209	0.04768

Fig. 2 shows the FESEM images of pure ZnO (a, b) and 1.0 at.% La-doped ZnO (c, d) samples. It is obvious that the morphology of pure ZnO shows an inhomogeneous and irregular elliptical shape with a diameter about 200~400 nm. However, the particles change into a fairly uniform, homogeneous spherical shape with an average particle size of 40~50 nm for the doped ZnO. The significant effect of La doping is observed on the microstructures of ZnO powders, demonstrating that lanthanum incorporation can dramatically decrease the particle size and change the morphology of ZnO [22].

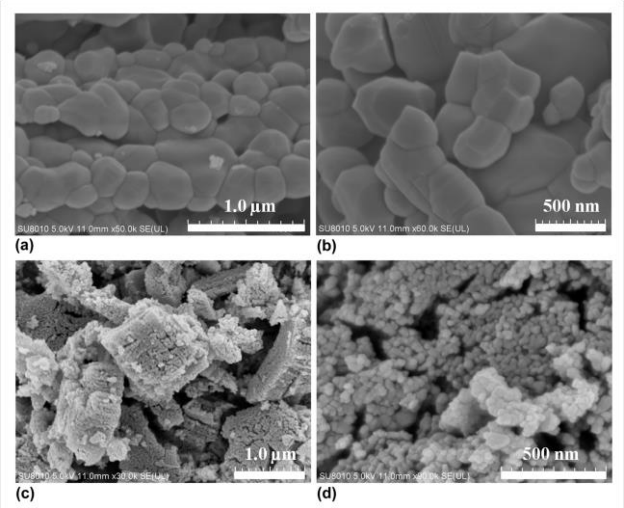

Fig. 2. FESEM images of pure ZnO (a, b) and 1.0 at.% La-doped ZnO (c, d) samples.

The surface composition and valence states of 1.0 at.% La-doped ZnO NSs were investigated by XPS measurement as shown in Fig. 3(a). All binding energies have been corrected for the charging effect with the C 1s reference at 284.6 eV. The core level XPS spectrum of Zn 2p is observed in Fig. 3(b). The two sharp peaks centering at 1021.1 eV and 1044.2 eV are assigned to the two spin-orbit components of Zn $2p_{3/2}$ and Zn $2p_{1/2}$ in ZnO, respectively. The La 3d spectrum exhibits four peaks with binding energy values of 834.7, 838.6, 851.3 and 855.7 eV in Fig. 3(c), which proves the existence of La–O bonds [26]. Because the appearance of satellite peaks associated to La 3d is related to the formation of lanthanum oxide. Moreover, consulting the literature [22], La $3d_{5/2}$ and La $3d_{3/2}$ peaks correspond to the peak of La^{3+}, which reveals that La exists mainly in the 3+ valence state in the sample. The O 1s spectrum in Fig. 3(d) shows a broad and unsymmetrical peak centering at 530.0 eV, indicating that oxygen bound to the surface of La-doped ZnO sample has different chemical states. The O 1s peak can be fitted into two peaks centering at about 529.8 eV and 531.3 eV, respectively. Since La^{3+} ions incorporated in the ZnO can make interaction with oxidic sites of ZnO, the peak located at 531.3 eV could be mainly assigned to the existence of Zn–O–La bond while that at 529.8 eV can be attributed to the lattice oxygen (Zn–O–Zn).

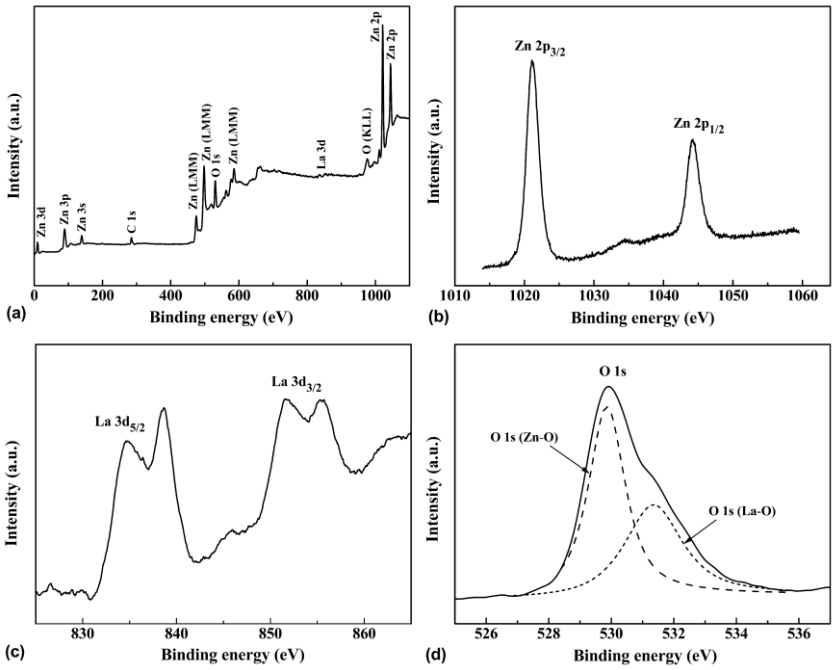

Fig. 3. (a) XPS spectra of 1.0 at.% La-doped ZnO particles and the high-resolution spectra of (b) Zn 2p, (c) La 3d, and (d) O 1s.

3.2. Optical characteristics

Fig. 4 shows the UV-vis absorption spectra of La-doped ZnO with various doping concentrations measured between 250~800 nm. It is obvious that all the samples perform relatively high transparency in the visible range. Sharp absorption edges can be clearly seen at about 380 nm in the ultraviolet range, implying ZnO is a kind of UV-shielding material [27]. It can be seen that La incorporation improves the optical absorption of ZnO for the doping concentrations below 1.5 at.%. However, the sample with a minor phase of La_2O_3 exhibits a weaker absorption performance than pure ZnO. This is because the La_2O_3 separated from the main phase covers the surface of ZnO particles and inhibits the direct exposure of the sample to the UV light [18].

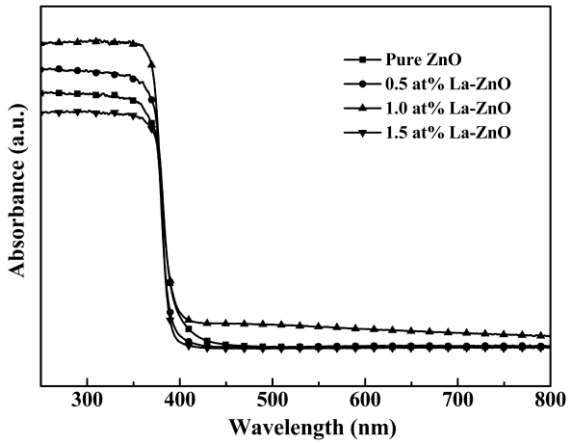

Fig. 4. UV-vis absorption spectra of La-doped ZnO with various doping concentrations.

For the direct band gap semiconductor, we can estimate the band gap of all the La doped ZnO NSs from the linear fit in the plot of $(\alpha h\nu)^2$ versus $h\nu$, where α is the absorption coefficient and $h\nu$ is the photo energy. Then extrapolate of the linear portion of $(\alpha h\nu)^2$ to zero to get the band gap E_g of the samples [28].

With the formula, the band gap of pure ZnO and La-doped ZnO can be calculated as presented in Fig. 5. It can be noted that the E_g value of pure ZnO is about 3.163 eV while that of La doped ZnO samples (0.5, 1.0, and 1.5 at.%) are 3.174, 3.181 and 3.191 eV, respectively. The band gap energy of the samples increases with the La content, which can be ascribed to the Burstein-Moss effect [29, 30]. The incorporation of La^{3+} into ZnO can provide additional free carriers, which causes the Fermi level to move into the conduction band, and finally promotes the absorption edge to shift to higher energy. The enhanced band gap energy could also be correlated with the quantum size effect, attributed to the reduction of crystallite size [31]. Furthermore, the appearance of La_2O_3 (E_g = 5.5 eV) is another reason for the band gap energy increase of 1.5 at.% La-doped ZnO sample [32].

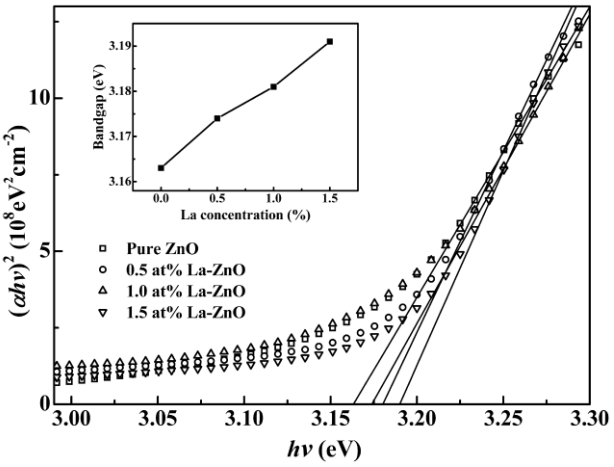

Fig. 5. The band gap of La-doped ZnO with various doping concentrations. Inset is the image of the band gap versus the La content, respectively.

3.3. Photocatalytic activity

Fig. 6(a) illustrates the variation of absorption spectra of MO aqueous solution in the presence of 1.0 at.% La-doped ZnO NSs. It can be seen that the characteristic absorbance peak of MO at 464 nm gradually decreases under UV irradiation. And the color of the suspension gradually becomes lighter, concomitantly. When the irradiation time reaches 180 min, the characteristic absorbance peak almost disappears, which implies that the chromophoric structure of MO has been almost completely destroyed. Fig. 6(b) depicts the comparison between different photocatalytic degradation activities of MO aqueous solution in the presence of La-doped ZnO with various doping concentrations. C_0 and C_t are the concentration of MO before and after irradiation, respectively. It can be observed that the concentration of MO aqueous solution without any catalyst remains unchanged under the UV light irradiation. Due to its stability, the photocatalytic degradation of MO under UV irradiation is used to evaluate the photocatalytic activities of both pure ZnO and La-doped ZnO samples.

According to the curves in Fig. 6(b), pure ZnO has shown its lower photocatalytic efficiency and merely 65% MO dyes are decomposed within 180 min, while its doped counterparts have exhibited significant enhancements (> 92%). The photocatalytic degradation efficiency of the samples can be arranged as follows: 1.0 at.% > 0.8 at.% > 0.5 at.% > 0.2 at.% >1.5 at.% La doped ZnO > pure ZnO. The following reasons can be regarded as possible explanations for this result. With the broadening of band gap for La-doped ZnO NSs, the edge of the conduction band would become more negative and the edge of the valence band would be more positive. As a result, the photogenerated electrons and holes have stronger redox ability and thus more highly reactive radicals can be produced in the surface of ZnO, which helps facilitate the photocatalytic degradation [33-35]. Moreover, La-doped ZnO NSs with the uniform nanoscale surface morphology would provide more chances for the encounter of the photogenerated electron-hole pairs with the MO molecules [36]. Furthermore, the nanosphere structure favors the transfer of electrons and holes generated inside the crystal to the surface [37], which also contributes to the enhanced photocatalytic activity of La-doped ZnO NSs. However, further increase of La^{3+} incorporation results in a decrease in the photocatalytic performance. This can be clearly observed from the present study that 1.5 at.% La-doped ZnO shows a lower photocatalytic activity than other doped samples. This is probably due to the fact that the excess La_2O_3 covering the surface of ZnO particles may inhibit direct UV light illumination, which further obstructs the transfer of photo-generated electrons to the conduction band and increases the number of recombination centers for electrons and holes, thus reducing the photocatalytic activity [18].

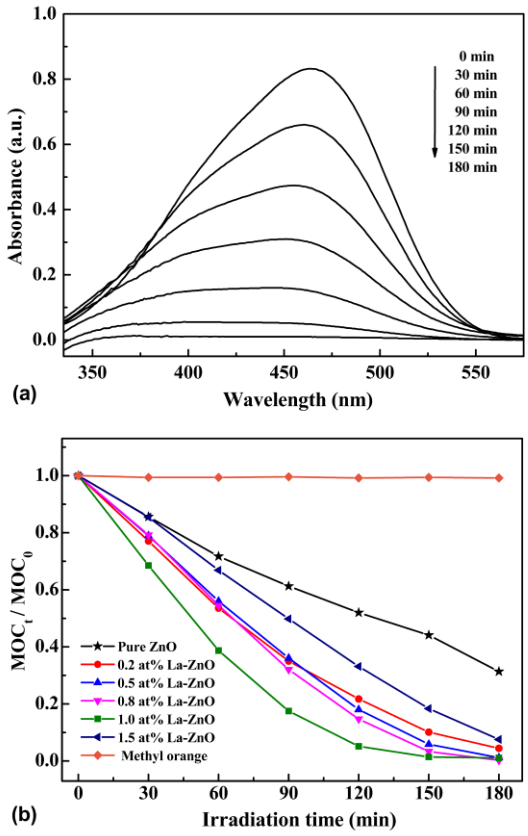

Fig. 6. (a) Absorption spectra of MO aqueous solution in the presence of 1.0 at.% La-doped ZnO sample under UV light for different irradiation time; (b) Comparison of the photocatalytic degradation activity of MO aqueous solution using La-doped ZnO with various doping concentrations as catalysts.

4. Conclusions

Pure ZnO and doped ZnO nanospheres with different La content were successfully synthesized by a two-step facile co-precipitation method under the open system. The catalysts with La^{3+} incorporation were found to exhibit notably enhanced photocatalytic performance in comparison with the undoped ZnO. The photocatalytic efficiency of the samples rose accordingly as the content increased, and the optimal dopant content is 1.0 at.%. The uniform nanoscale surface morphology enhanced the absorption capability and the increased band gap caused by La^{3+} incorporation promoted the generation of highly reactive radicals in the surface of ZnO. Therefore, it can be concluded that La doping has a significant impact on improving the photocatalytic performance of ZnO, and La-doped ZnO NSs can be served as a promising photocatalyst for the degradation of toxic dyestuffs in the aquatic environment.

Acknowledgements

We gratefully acknowledge funding from the National Natural Science Foundation of China (grant nos. 41172051 and 40872039), the Fundamental Research Founds for National University (grant no. 1410491B04), the National College Students' Innovative Training Program (grant no. 201210491020) and the Teaching Laboratory Opening Funds (grant nos. SKJ2012182 and SKJ2013012), China University of Geosciences (Wuhan).

References

[1] A. R. Khataee, V. Vatanpour, A. R. Amani Ghadim, J. Hazard. Mater. **161**, 1225 (2009).
[2] F. Han, V. S. R Kambala, M. Srinivasan, D. Rajarathnam, R. Naidu, Appl. Catal. A **359**, 25 (2009).
[3] T. T. Miao, Y. R. Guo, Q. J. Pan, J. Nanopart. Res. **15**, 1725 (2013).
[4] M. Ahmad, E. Ahmed, Y. W. Zhang, N.R. Khalid, J. F. Xu, M. Ullah, Z. L. Hong, Curr. Appl. Phys. **13**, 697 (2013).
[5] O. Carp, C. L. Huisman, A. Reller, Prog. Solid State Chem. **32**, 33 (2004).
[6] X. W. Duan, G. Z. Wang, H. Q. Wang, Y. Q. Wang, C. Shen, W. P. Cai, CrystEngComm **12**, 2821 (2010).
[7] U. I. Gaya, A. H. Abdullah, M. Z. Hussein, Z. Zainal, Desalination **263**, 176 (2010).
[8] C. G. Tian, Q. Zhang, B. J. Jiang, G. H. Tian, H. G. Fu, J. Alloys Compd. **509**, 6953 (2011).
[9] F. Xu, Y. F. Yuan, D. P. Wu, M. Zhao, Z. Y. Gao, K. Jiang, Mater. Res. Bull. **48**, 2066 (2013).
[10] Y. Zheng, L. Zheng, Y. Zhan, X. Lin, Q. Zheng, K. Wei, Inorg. Chem. **46**, 6980 (2007).
[11] A. Mclaren, T. Valdes-Solis, G. Q. Li, S. C. Tsang, J. Am. Chem. Soc. **131**, 12540 (2009).
[12] F. Z. Sun, X. L. Qiao, F. T. Tan, W. Wang, X. L. Qiu, J. Mater. Sci. **47**, 7262 (2012).
[13] B. P. Nenavathua, A. K. Rao, A. Goyal, A. Kapoor, R. K. Dutta, Appl. Catal., A **459**, 106 (2013).
[14] M. M. Ba-Abbad, A. A. H. Kadhum, A. B. Mohamad, M. S. Takriff, K. Sopian, Chemosphere **91**, 1604 (2013).
[15] H. B. Lu, H. Li, L. Liao, Y. Tian, M. Shuai, J. C. Li, M. F. Hu, Q. Fu, B. P. Zhu, Nanotechnology **19**, 045605 (2008).
[16] W.E. Mahmoud, J. Cryst. Growth **312**, 3075 (2010).
[17] C. Q. Ge, C. S. Xie, M. L. Hu, Y. H. Gui, Z. K. Bai, D. W. Zeng, Mater. Sci. Eng. B **141**, 43 (2007).
[18] S. Anandan, A. Vinu, T. Mori, N. Gokulakrishnan, P. Srinivasu, V. Murugesan, K. Ariga, Catal. Commun. **8**, 1377 (2007).
[19] S. Anandan, Y. Ikuma, V. Murugesan, Int. J. Photoenergy. doi: 10.1155/2012/921412 (2012).
[20] A. Kajbafvala, H. Ghorbani, A. Paravar, J. P.

Samberg, E. Kajbafvala, S. K. Sadrnezhaad, Superlattices Microstruct. **51**, 512 (2012).
[21] M. S. Mohajerani, A. Lak, A. Simchi, J. Alloys Compd. **485**, 616 (2009).
[22] J. T. Chen, J. Wang, F. Zhang, G. A. Zhang, Z. G. Wu, P. X. Yan, J. Cryst. Growth **310**, 2627 (2008).
[23] R. Yogamalar, S. Anitha, R. Srinivasan, A. Vinu, K. Ariga, A. C. Bose, J. Nanosci. Nanotechno. **9**, 5966 (2009).
[24] T. Ahmad, S. Vaidya, N. Sarkar, S. Ghosh, A. K. Ganguli, Nanotechnology **17**, 1236 (2006).
[25] S. Suwanboon, P. Amornpitoksuk, Ceram. Int. **37**, 3515 (2011).
[26] H. Berthou, C. K. Jørgensen, C. Bonnello, Chem. Phys. Lett. **38**, 199 (1976).
[27] Y. Q. Li, S. Y. Fu, Y. W. Mai, Polymer **47**, 2127 (2006).
[28] Y. Z. Zhang, L. H. Wu, H. Li, J. H. Xu, L. Z. Han, B. C. Wang, Z. L. Tuo, E. Q. Xie, J. Alloys Compd. **473**, 319 (2009).
[29] S. H. Deng, M. Y. Duan, M. Xu, L. He, Physica B **406**, 2314 (2011).
[30] T. Rattana, S. Suwanboon, P. Amornpitoksuk, A. Haidoux, P. Limsuwan, J. Alloys Compd. **480**, 603 (2009).
[31] L. Q. Jing, X. J. Sun, B. F. Xin, B. Q. Wang, W. M. Cai, H. G. Fu, J. Solid State Chem. **177**, 3375 (2004).
[32] W. Lan, Y. P. Liu, M. Zhang, B. Wang, H. Yan, Y. Y. Wang, Mater. Lett. **61**, 2262 (2007).
[33] T. J. Sun, J. S. Qiu, C. H. Liang, J. Phys. Chem. C **112**, 715 (2008).
[34] W. J. Zhou, Y. H. Leng, D. M. Hou, H. D. Li, L. G. Li, G. Q. Li, H. Liu, S. W. Chen, Nanoscale **6**, 4698 (2014).
[35] Z. H. Li, Z. P. Xie, Y. F. Zhang, L. Wu, X. X. Wang, X. Z. Fu, J. Phys. Chem. C **111**, 18348 (2007).
[36] F. Xu, D. F. Guo, H. J. Han, H. X. Wang, Z. Y. Gao, D. P. Wu, K. Jiang, Res. Chem. Intermed. **38**, 1579 (2012).
[37] W. W. Wang, Y. J. Zhu, L. X. Yang, Adv. Funct. Mater. **17**, 59 (2007).

*Corresponding author: dwmeng@cug.edu.cn
wuxiuling830@163.com